

# High quality factor nitride-based optical cavities: microdisks with embedded GaN/Al(Ga)N quantum dots

M. Mexis,<sup>1</sup> S. Sergent,<sup>2,3</sup> T. Guillet,<sup>1,\*</sup> C. Brimont,<sup>1</sup> T. Bretagnon,<sup>1</sup> B. Gil,<sup>1</sup> F. Semond,<sup>2</sup> M. Leroux,<sup>2</sup> D. Néel,<sup>4</sup> S. David,<sup>4</sup> X. Chécoury,<sup>4</sup> and P. Boucaud<sup>4</sup>

<sup>1</sup>Laboratoire Charles Coulomb, UMR5221, CNRS/UM2, Université Montpellier 2, F-34095, Montpellier, France

<sup>2</sup>Centre de Recherche sur l'Hetero-Epitaxie et ses Applications - CNRS, 06560, Valbonne, France

<sup>3</sup>Université de Nice Sophia Antipolis, Parc Valrose, 06102, Nice, France

<sup>4</sup>Institut d'Electronique Fondamentale, CNRS—Université Paris Sud, 91405, Orsay, France

\*Corresponding author: thierry.guillet@univ-montp2.fr

Received January 20, 2011; revised May 6, 2011; accepted May 6, 2011;

posted May 10, 2011 (Doc. ID 139867); published June 7, 2011

We compare the quality factor values of the whispering gallery modes of microdisks ( $\mu$ -disks) incorporating GaN quantum dots (QDs) grown on AlN and AlGaN barriers by performing room temperature photoluminescence (PL) spectroscopy. The PL measurements show a large number of high  $Q$  factor resonant modes on the whole spectrum, which allows us to identify the different radial mode families and to compare them with simulations. We report a considerable improvement of the  $Q$  factor, which reflects the etching quality and the relatively low cavity loss by inserting QDs into the cavity. GaN/AlN QDs-based  $\mu$ -disks show very high  $Q$  values ( $Q > 7000$ ) whereas the  $Q$  factor is only up to 2000 in  $\mu$ -disks embedding QDs grown on the AlGaN barrier layer. We attribute this difference to the lower absorption below bandgap for AlN barrier layers at the energies of our experimental investigation. © 2011 Optical Society of America

OCIS codes: 230.3990, 230.5590, 230.7020, 250.5230, 300.6320, 350.4238.

III-N semiconductors have attracted much attention for the fabrication of UV and visible light sources covering a wide range of applications. Thus, a great effort has been made for realizing low threshold and high performance laser devices operating at room temperature. This has shifted the interest toward new directions, such as: (i) the fabrication of low-dimensional systems in order to reduce the nonradiative mechanisms generally taking place in bulk materials, especially at 300 K, and (ii) the control of their coupling to light through photonic structures aiming at improving the emission and collection efficiencies. Such cavities have previously been successfully implemented for N-based materials, and optical modes of high  $Q$  values ( $Q = \lambda/\delta\lambda$ ) have been reported up to  $Q \sim 4000$  [1–3]. However, mastering the technology for nitride photonic structures dedicated to UV applications is far more challenging than that of technologically more established materials emitting in IR. This is related to their size, which scales down with the wavelength of emission, and also to the chemical inertness of III-N materials. Microdisks ( $\mu$ -disks) are interesting photonic structures for N-based materials [4], sustaining low mode volume and high  $Q$  factor whispering gallery modes (WGMs) [5], and also being well adapted to the demonstration of low-threshold laser operation [3,6,7].

Quantum dots (QDs) are promising emitters to be embedded in photonic cavities. With respect to the observation of the photonic modes, an interesting feature of QDs compared to quantum wells (QWs) is that they present a larger inhomogeneous broadening. Thus, they allow probing a wide range of cavity modes. Moreover, the optical losses within the cavity can be reduced due to the relatively low absorption of light by dots [8]. In addition, QDs have also allowed the observation of phenomena such as strong light–matter coupling [9] and the Purcell

effect [8,10], leading to new low-threshold QD lasers [11,12]. Recent results about GaN/(Al,Ga)N QDs grown on Si have shown that their photoluminescence (PL) remains intense even at 300 K [13] due to the strong quantum confinement of carriers.

In this work we report considerable improvement of the optical quality of  $\mu$ -disks with embedded GaN/AlN QDs. By performing micro-PL ( $\mu$ -PL) measurements, we compare the WGMs and the  $Q$  factors of various disk diameters containing GaN QDs grown on two different barrier layers, namely AlN and (Al,Ga)N. The large number of observed WGMs allows identifying the different radial order families of modes and comparing them with simulations.

The QD samples are grown by ammonia-based molecular beam epitaxy. The main studied sample, shown in Fig. 1(a), consists of a stack of four GaN/AlN QD planes. The first QD plane is nucleated on a 35 nm-thick AlN buffer layer grown on a Si(111) substrate. The four QD planes are separated by 10 nm-thick AlN spacers and the last plane is capped by a 35 nm-thick AlN layer. The second sample is constituted of a 15 nm AlN buffer layer followed by a 35 nm  $\text{Al}_{0.5}\text{Ga}_{0.5}\text{N}$  layer, on top of which is grown a GaN QD plane. The QD plane is finally capped by a 50 nm  $\text{Al}_{0.5}\text{Ga}_{0.5}\text{N}$  layer.

The limited thickness, 110 nm, of the nitride-based slab for both samples allows us to use the optical active area as a single mode waveguide in the  $\mu$ -disk plane (details in [4,13]). The diameter of the studied  $\mu$ -disks was varied from 2 to 5  $\mu\text{m}$ . The scanning electron microscope (SEM) image in Fig. 1(b) shows a 2  $\mu\text{m}$  diameter  $\mu$ -disk sitting on top of a Si post. The etching quality, deduced from the SEM image, is very high and this is further confirmed by performing optical characterization detailed below.

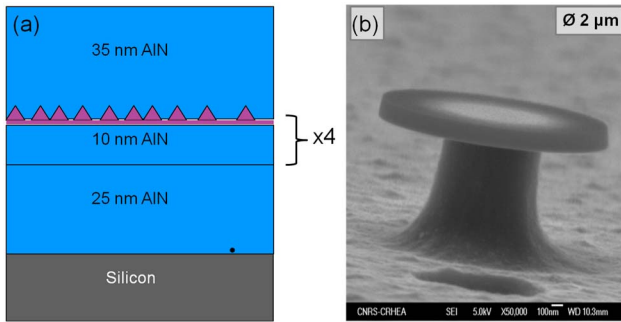


Fig. 1. (Color online) (a) Epitaxial structure, the optical active area above the Si substrate contains four periods of GaN/AlN QDs layers. (b) SEM image of a  $2\ \mu\text{m}$  in diameter  $\mu$ -disk.

Our microscopy setup allows us to photo-excite a single  $\mu$ -disk with a 266 nm CW laser (Crylas/FQCW 266-50). The spot diameter is  $1.5\ \mu\text{m}$ . The  $\mu$ -PL present here is collected from the edge of the sample parallel to the  $\mu$ -disk plane within which the WGMs are propagating, with a spectral resolution of  $\sim 0.16\ \text{meV}$ .

In Fig. 2, we present PL spectra for  $\mu$ -disks of various radii with embedded GaN/AlN and GaN/(Al,Ga)N dots. For disks incorporating GaN/AlN dots [Figs. 2(a) and 2(b)], sharp peaks uniformly and periodically spaced appear across each spectrum, corresponding to WGMs that are distinguishable within a wide spectral range from 2.6 to 3.4 eV. We wish to emphasize that such a uniformity of the WGMs across the whole spectrum as well as the fact that these modes are clearly distinguishable for a wide spectral range has not been reported until now in any nitride-based  $\mu$ -disk. Indeed, in the case of  $\mu$ -disk embedding QWs, the modes are clearly observed only at the low energy side of the spectrum due to reabsorption by the QW states at higher energy [7].

For the  $\mu$ -disks incorporating GaN/AlN dots, the  $Q$  factor reaches a maximum value of  $\sim 5000$  for the  $2\ \mu\text{m}$  diameter  $\mu$ -disk and  $\sim 7300$  for the  $5\ \mu\text{m}$  one [inset of Fig. 2(b)]. To our knowledge, these  $Q$  values are state of the art for nitride photonic structures and we attribute this achievement to the high etching quality of the  $\mu$ -disk and to the low absorption of dots as compared to wells. In the case of (Al,Ga)N-based  $\mu$ -disks [Fig. 2(c)], the  $Q$  values are measured smaller by a factor more than three times that of AlN ones. The deterioration of the  $Q$  factor is attributed to the larger residual absorption of the (Al, Ga)N barriers in the spectral range investigated here, which is not only related to the lower bandgap energy of such barriers but also to the lower crystal quality, especially due to alloy disorder [14].

Within the  $\mu$ -disk the WGMs are described by the azimuthal number  $m$  and the radial number  $n$  of Bessel functions [5] while the field outside the dielectric is described by Henkel functions. In order to identify the different families of modes (i.e., modes of the same radial number  $n$ ) from  $\mu$ -PL spectra, we analyze in Fig. 3 both the  $Q$  factor of each mode and the free spectral range (FSR) of each family of modes. The experimental findings are compared with those of a theoretical model based first on the calculation of the guided modes in a standard planar one-dimensional waveguide [15] and then on solving the Maxwell equations across a boundary of cylindrical symmetry [16]. Because of the thickness of

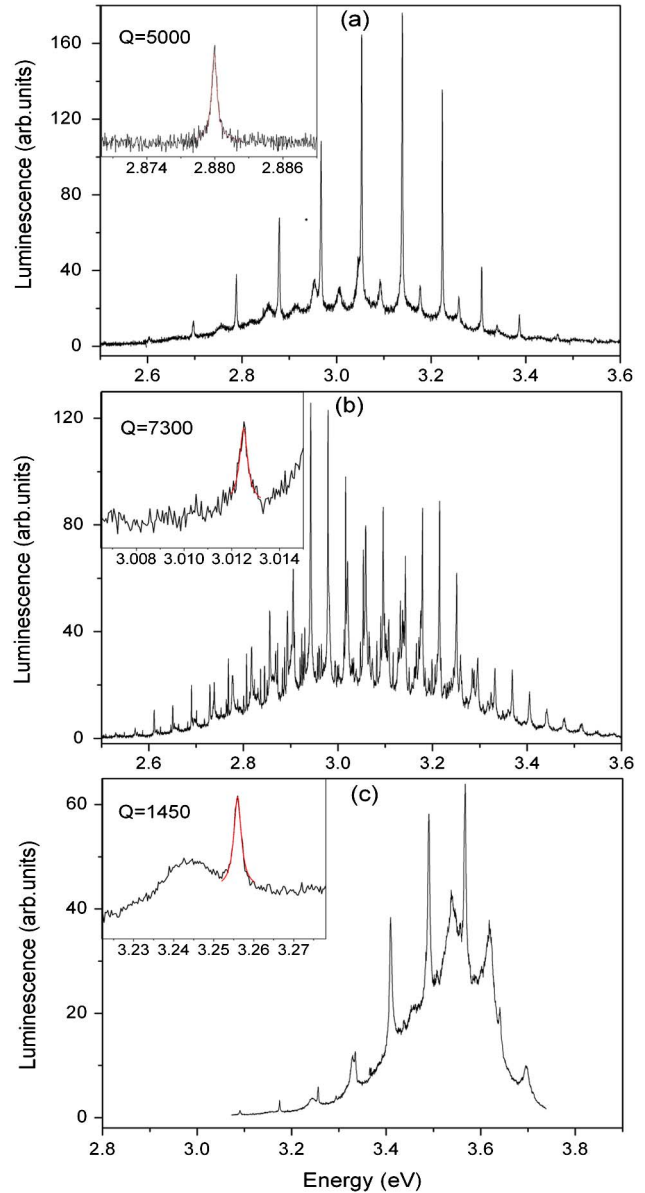


Fig. 2. (Color online) Room temperature PL spectra (excitation power density  $\sim 60\ \text{W}/\text{cm}^2$ ) of (a), (c)  $2\ \mu\text{m}$  and (b)  $5\ \mu\text{m}$  in diameter  $\mu$ -disks with embedded (a), (b) GaN/AlN and (c) GaN/AlGaIn dots presented within similar spectral range  $\sim 1.1\ \text{eV}$ . Insets, high resolution spectra showing the WGM with the highest  $Q$  value.

the slab waveguide, typically of a half wavelength in size, only the fundamental order modes are calculated, taking into account the spectral dependence of the effective refractive index. The polarization of the observed WGM is predominantly the TE polarization so we have only considered TE modes here.

Figure 3(a) presents the  $Q$  values of the sharpest modes that appear within a clear periodic way across the whole  $\mu$ -PL spectrum of Fig. 2(a). For the  $2\ \mu\text{m}$   $\mu$ -disk, we assign the different radial mode families by both considering modes with similar  $Q$  factors and similar FSRs. In Fig. 3(b), we compare the FSRs of these modes to the ones estimated by the model. A good agreement with the model is found for a  $\mu$ -disk of diameter  $d = 2.06\ \mu\text{m}$  close to the nominal value. From the graph we can distinguish the two

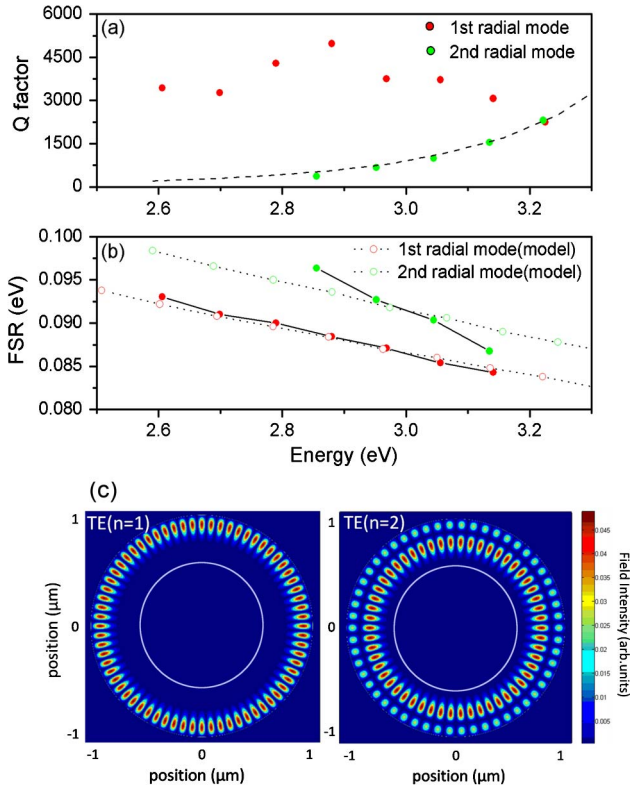


Fig. 3. (Color online) (a)  $Q$  values of the first and the second radial order families of WGMs for a  $\sim 2\ \mu\text{m}$   $\mu$ -disk; the dashed line is proportional to the inverse of the overlap of the second radial mode with the post that limits their  $Q$  factor (b) FSR of the two mode families (full circles). Theoretical values are shown in open circles. (c) An example of simulated first (left) and second (right) radial order modes for a  $2.06\ \mu\text{m}$ -diameter  $\mu$ -disk showing the TE field distribution within the disk plane (the light gray open circle represents the  $\mu$ -disk post periphery).

first radial mode families,  $n = 1$  and  $n = 2$ . First-order modes ( $n = 1$ ) show the highest  $Q$  values because they propagate closer to the periphery of the disk whereas  $n = 2$  modes propagate closer to the center of the post where absorption reduces their  $Q$  values by a factor related to their spatial overlap with the post [Fig. 3(a)]. Thus modes of higher  $n$ , i.e.  $n > 2$ , are not periodically observed along the PL spectrum because they are damped by absorption. Both the spatial position and the degree of confinement of the first two radial order modes within the disk plane can be observed in Fig. 3(c), showing an example of the simulated field distribution of  $n = 1, 2$  WGMs.

Within the  $\mu$ -disk microcavities studied here, the limitations of the WGM  $Q$  values are described by [6]

$$Q^{-1} = Q_{\text{rad}}^{-1} + Q_{\text{scat}}^{-1} + Q_{\text{abs}}^{-1}, \quad (1)$$

where the two first factors  $Q_{\text{rad}}^{-1}$  and  $Q_{\text{scat}}^{-1}$  are related to photons leaking outside the cavity as photons radiate outside the cavity ( $Q_{\text{rad}}^{-1}$ ) or get scattered ( $Q_{\text{scat}}^{-1}$ ) due to imperfections that have been induced at the disk periphery during the etching process. The last factor is given by [6]

$$Q_{\text{abs}}^{-1} = \frac{\alpha\lambda}{2\pi n_{\text{eff}}}, \quad (2)$$

where  $\alpha$  is the mean absorption coefficient and  $n_{\text{eff}}$  is the effective refractive index of the WGM. For both materials,

the  $Q_{\text{rad}}^{-1}$  and  $Q_{\text{scat}}^{-1}$  values that are respectively estimated from the  $\mu$ -disk geometry and the roughness of the  $\mu$ -disk sidewalls [16], respectively, are calculated to be higher than  $10^4$  through the whole spectral range [13]. Thus the main mechanism responsible for optical losses is absorption ( $Q_{\text{abs}}^{-1}$ ) in the silicon post or in the optical active area.

We have shown that for the  $\mu$ -disks containing GaN dots grown on AlN layers, we can achieve with  $Q$  factors of values more than three times higher than those with dots grown on AlGaIn layer. We attribute this decrease of  $Q$  factor for the latter sample to absorption in AlGaIn barrier layers. For  $\mu$ -disks embedding GaN/AlN dots, we have demonstrated high  $Q$  values up to  $Q \sim 7300$ . This improvement of the  $Q$  value is associated with the etching quality and with the relatively low cavity loss by inserting dots into the cavity. The wide spectral PL emission of QDs at 300 K allows us to identify the first two radial order mode families,  $n = 1, 2$ , by comparing their FSR to simulations.

The authors thank B. Gayral and D. Sam-Giao for their helpful discussion. This work is supported by the French Agence Nationale de la Recherche (research program SINPHONI ANR-08-NANO-021-01).

## References

1. E. D. Haberer, R. Sharma, C. Meier, A. R. Stonas, S. Nakamura, S. P. DenBaars, and E. L. Hu, *Appl. Phys. Lett.* **85**, 5179 (2004).
2. M. Arita, S. Ishida, S. Kako, S. Iwamoto, and Y. Arakawa, *Appl. Phys. Lett.* **91**, 051106 (2007).
3. D. Simeonov, E. Feltin, H. J. Bühlmann, T. Zhu, A. Castiglia, M. Mosca, J. F. Carlin, R. Butté, and N. Grandjean, *Appl. Phys. Lett.* **90**, 061106 (2007).
4. S. Sergent, J. C. Moreno, E. Frayssinet, Y. Laaroussi, S. Chenot, J. Renard, D. Sam-Giao, B. Gayral, D. Néel, S. David, P. Boucaud, M. Leroux, and F. Semond, *J. Phys. Conf. Ser.* **210**, 012005 (2010).
5. S. L. McCall, A. F. J. Levi, R. E. Slusher, S. J. Pearton, and R. A. Logan, *Appl. Phys. Lett.* **60**, 289 (1992).
6. R. E. Slusher, A. F. J. Levi, U. Mohideen, S. L. McCall, S. J. Pearton, and R. A. Logan, *Appl. Phys. Lett.* **63**, 1310 (1993).
7. A. C. Tamboli, E. D. Haberer, R. Sharma, K. H. Lee, S. Nakamura, and E. L. Hu, *Nat. Photon.* **1**, 61 (2007).
8. B. Gayral, J. M. Gérard, A. Lemaître, C. Dupuis, L. Manin, and J. L. Pelouard, *Appl. Phys. Lett.* **75**, 1908 (1999).
9. T. Yoshie, A. Scherer, J. Hendrickson, G. Khitrova, H. M. Gibbs, G. Rupper, C. Ell, O. B. Shchekin, and D. G. Deppe, *Nature* **432**, 200 (2004).
10. J. M. Gerard and B. Gayral, *J. Lightwave Technol.* **17**, 2089 (1999).
11. F. Bordas, C. Seassal, E. Dupuy, P. Regreny, M. Gendry, P. Viktorovitch, M. J. Steel, and A. Rahmani, *Opt. Express* **17**, 5439 (2009).
12. S. Strauf, K. Hennessy, M. T. Rakher, Y. S. Choi, A. Badolato, L. C. Andreani, E. L. Hu, P. M. Petroff, and D. Bouwmeester, *Phys. Rev. Lett.* **96**, 127404 (2006).
13. S. Sergent, J. C. Moreno, E. Frayssinet, S. Chenot, M. Leroux, and F. Semond, *Appl. Phys. Express* **2**, 051003 (2009).
14. D. Brunner, H. Angerer, E. Bustarret, F. Freudenberg, R. Höppler, R. Dimitrov, O. Ambacher, and M. Stutzmann, *J. Appl. Phys.* **82**, 5090 (1997).
15. A. Yariv, *Optical Electronics*, 4th ed. (Saunders College Publishing, 1995).
16. M. Borselli, T. Johnson, and O. Painter, *Opt. Express* **13**, 1515 (2005).